RSC Advances

PAPER

View Article Online
View Journal | View Issue

Cite this: *RSC Adv.*, 2019, **9**, 1642

Production of green biofuel by using a goat manure supported Ni–Al hydrotalcite catalysed deoxygenation process

Shajaratun Nur Zdainal Abidin,[a] Hwei Voon Lee, *[a] Joon Ching Juan, [a] Noorsaadah Abd Rahman[b] and Yun Hin Taufiq-Yap[c]

The high oxygen content in natural biomass resources, such as vegetable oil or biomass-pyrolysed bio oil, is the main constraint in their implementation as a full-scale biofuel for the automotive industry. In the present study, renewable fuel with petrodiesel-like properties was produced *via* catalytic deoxygenation of oleic acid in the absence of hydrogen (H_2). The deoxygenation pathway of oleic acid to bio-hydrocarbon involves decarboxylation/decarbonylation of the oxygen content from the fatty acid structure in the form of carbon dioxide (CO_2)/carbon monoxide (CO), with the presence of a goat manure supported Ni–Al hydrotalcite (Gm/Ni–Al) catalyst. Goat manure is an abundant bio-waste, containing a high mineral content, urea as well as cellulosic fiber of plants, which is potentially converted into activated carbon. Synthesis of Gm/Ni–Al was carried out by incorporation of pre-activated goat manure (GmA) during co-precipitation of Ni–Al catalyst with 1 : 3, 1 : 1 and 3 : 1 ratios. The physico-chemical properties of the catalysts were characterized by X-ray diffractometry (XRD), Brunauer–Emmet–Teller (BET) surface area, field emission surface electron microscopy (FESEM) and temperature program desorption ammonia (TPD-NH_3) analysers. The catalytic deoxygenation reaction was performed in a batch reactor and the product obtained was characterized by using gas chromatography-mass spectroscopy (GCMS) for compound composition identification as well as gas chromatography-flame ionisation detector (GC-FID) for yield and selectivity determination. The optimization and evaluation were executed using response surface methodology (RSM) in conjunction with central composite design (CCD) with 5-level-3-factors. From the RSM reaction model, it was found that the Gm/Ni–Al 1 : 1 catalysed deoxygenation reaction gives the optimum product yield of 97.9% of hydrocarbon in the range of C_8–C_{20}, with diesel selectivity (C_{17}: heptadecane and heptadecene compounds) of 63.7% at the optimal reaction conditions of: (1) reaction temperature: 327.14 °C, (2) reaction time: 1 h, and (3) catalyst amount: 5 wt%.

Received 20th September 2018
Accepted 16th December 2018

DOI: 10.1039/c8ra07818a

rsc.li/rsc-advances

Introduction

It is generally known that massive fossil fuel utilization has led to critical environmental devastation. In addition, it is also a non-renewable and non-biodegradable product, which can possibly diminish over time.[1,2] Biofuel, derived from plants or biomass, has been considered as a fossil fuel substitute for decades. It can be easily produced by several methods: (1) transesterification/esterification of triglycerides to produce biodiesel/bioethanol, (2) pyrolysis of biomass to produce short chain hydrocarbon products known as bio-oil, and (3) deoxygenation/hydrodeoxygenation of oil to produce paraffinic hydrocarbons.[3–5] Fuels produced using methods (1) and (2) have been reported as promising petroleum fuel substitutes; however, the high volume of oxygen in the products leads to (i) fuel degradation, resulting from incomplete combustion and (ii) deposition of carbon in the fuel engine. Eventually, the carbon deposition causes engine clogging, preventing it from running smoothly. Moreover, fuels made using methods (1) and (2) are not compatible to be used directly in fuel engines without modification of the engine, hence, they need to be blended with petroleum fuel.[6,7]

To overcome these shortcomings, method (3) has been studied enormously by researchers.[8–10] Generally, hydrodeoxygenation (HDO) and deoxygenation (DO) are the same oxygen-removal process. Unfortunately, HDO consumes large amounts of hydrogen gas to produce more selective hydrocarbon products,[11,12] resulting in high operational costs. Despite being low in product selectivity, the DO reaction is more economical and practical to be implemented. HDO/DO reactions have been reported using various types of catalysts. Nobel

[a]*Nanotechnology & Catalysis Research Centre (Nanocat), Institute of Advance Studies, University of Malaya, 50603 Kuala Lumpur, Malaysia. E-mail: leehweivoon@um.edu.my; Fax: +603-79676959; Tel: +603-7957 6956*

[b]*Department of Chemistry, Faculty of Science, University of Malaya, 50603 Kuala Lumpur, Malaysia*

[c]*Catalysis Science & Technology Research Centre (PutraCAT), Faculty of Science, Universiti Putra Malaysia, 43400 UPM Serdang, Selangor, Malaysia*

metal-Ru, Rh, Pd, sulfided and zeolite catalysts are typically used for the HDO/DO reaction.[13–16] Nobel metal catalyst application is limited on an industrial scale owing to its expensive price. Sulfided catalyst leads to formation of undesirable sulfur-containing products, and is thus not in agreement with the demand for green fuel. The high acidity of zeolite-containing catalysts also results in a wide spectrum of products. This leads to the exploration of alkaline catalysed reactions, which proves that high basicity in catalysts is not only able to inhibit coke formation, but also improve the rate of the decarboxylation reaction mechanism.[17–19]

Hydrotalcite (HT), with the general formula of $[M(II)_{1-x}M(III)_x(OH)_2]^{x+}(A^{n-})_{x/n}\cdot mH_2O$, where M(II) and M(II) are divalent and trivalent metal cations, while A is intercalated anion, is a type of double layered hydroxide (LDH) catalyst that has basicity with ion exchange properties.[20–22] Typical hydrotalcite has strong alkaline content, which is derived from M(II) = Mg, which causes saponification of the high free fatty acid (FFA) feedstocks, thus the substitution of other active metals such as Ni was suggested. The interest in hydrotalcite as a catalyst has grown owing to its ability to be synthesized with various tunable basicity and acidity properties. It has been proved that hydrotalcite catalysts can catalyze HDO/HDO reactions, resulting in various paraffinic hydrocarbon products under severe reaction conditions (high pressure (100 psi) and temperature (350 °C)).[23–26] Ni also has a notorious ability in oil cracking, attributed to its high acidity of active sites.[27,28]

Goat manure is an abundant waste that is derived from plants consumed by goats, commonly grass. Owing to the high mineral content of goat manure, it is usually used as a fertilizer for planting purposes. Goat manure comprises urea as well as cellulosic fiber of plants, which can be converted to activated carbon. There are no studies that have been reported so far on using goat manure as a source of activated carbon. Besides, it has also never been used as a catalyst for biofuel production application. Thus, the aim of this study is to (1) synthesize and characterize a Gm/Ni–Al catalyst, (2) investigate the catalytic DO reaction of oleic acid over the Gm/Ni–Al catalyst, and (3) determine the optimum operating conditions by using response surface methodology (RSM), which leads to the maximum yield and diesel selectivity.

Experimental

Materials

Fresh goat manure was obtained from the local supplier, Bangi Malaysia. All metal salts for hydrotalcite synthesis: aluminium(III) nitrate nonahydrate, $Al(NO_3)_3\cdot 9H_2O$ (98.5%), nickel(II) nitrate hexahydrate, $Ni(NO_3)_2\cdot 6H_2O$ (97%) as well as sodium carbonate, Na_2CO_3 (99.5%), were obtained from R&M Chemicals Sdn. Bhd. Sodium hydroxide, NaOH (99%), was purchased from Merck. The internal standard 1-bromohexane, 1-CH_3Br (>98%), and the alkane and alkene standard solution (C_8–C_{20}) were purchased from Sigma-Aldrich. Hexane, GC Grade (>98%) was also obtained from Merck for dilution purposes. The oleic acid (99.5%) was acquired from QRec and the physicochemical properties of the oleic acid are tabulated in Table 1.

Table 1 Physicochemical properties of oleic acid

Properties	Description	Method
Oleic acid		
Molecular formula	$C_{18}H_{34}O_2$	
Decomposition temperature (°C)	239.37	TGA analysis
Density (g cm^{-3})	0.89	ASTM D1298
Viscosity at 40 °C (cSt)	4.5	ASTM D445-15a
Moisture content (wt%)	≤0.2	AOCS Ja 2b-87
Acid value (mg KOH per g)	196–204	AOCS Te 1a-64
FFA value (%)	98.5–102.5	AOCS Te 1a-64
Composition of oil (%)		GCMS analysis
Oleic acid	99.54	
Hydroperoxide	0.07	
n-Decanoic acid	0.03	
Dodecanoic acid	0.06	
Heptadecane	0.04	
n-Hexadecanoic acid	0.10	
9-Hexadecen-1-ol	0.15	

Preparation of catalyst

Fresh goat manure was dried in an oven for 48 h at 100 °C. Then it was ground to a powder and sieved. Next, the powdered goat manure was calcined at 300 °C for 20 min in a furnace with the presence of N_2 gas in order to activate the goat manure, denoted as Gm. Ni–Al HT catalyst supported on activated goat manure was synthesized by simple co-precipitation method.

The nickel salt ($Ni(NO_3)_2\cdot 6H_2O$) and aluminium salt ($Al(NO_3)_3\cdot 9H_2O$) were mixed up and dissolved in 250 ml of deionised water and Gm was added into the salt solution with Gm : Ni–Al molar ratios of 1 : 3, 1 : 1 and 3 : 1. The molar ratios of Gm to Ni–Al were calculated based on the moles of Gm to the sum of the moles of Ni–Al. A mixture of NaOH and Na_2CO_3 solution was prepared in a 1 : 1 molar ratio and dropped into the solution at a rate of 1 ml min^{-1} under vigorous stirring. Co-precipitation of the catalyst was carried out until the pH of the solution reached 11. The gelatinous precipitate formed was sonicated for 1 h and aged in an incubator shaker at 70 °C for 18 h. After the mixture was cooled to room temperature, it was filtered and washed with deionised water until pH 7 was obtained. The precipitate was dried in an oven and the obtained precursors were calcined at 500 °C for 3 h for activation, denoted as Gm/Ni–Al. Ni–Al HT catalyst was prepared by using the same co-precipitation method, but without the presence of Gm. The Ni–Al solution prepared with a ratio of 4 : 1 was precipitated out by pre-mixed NaOH and Na_2CO_3 solution. The physicochemical properties of all precursors and catalysts were characterized by X-ray diffractometry (XRD), Brunauer–Emmet–Teller (BET) surface area and temperature program desorption ammonia (TPD-NH_3) analysis.

Characterization of catalyst

XRD analysis was performed using a Shimadzu XRD-6000 Diffractometer at a scanning rate of 2° min^{-1} (2θ = 10–90°). The catalyst was scanned by Cu Kα radiation, generated by

a Philips glass diffraction X-ray tube (broad focus 2.7 kW type). The produced pattern was compared with Joint Committee on Powder Diffraction Standards (JCPDS) files. A Philips FEI Field Emission Scanning Electron Microscope model Quanta FEG 450 was used to capture the surface morphologies of the catalysts. Solid samples were coated with gold by a BIO-RAS Sputter before they were analysed. Images were then captured at scales of 1 and 0.1 μm. The specific surface area of the catalyst was determined by using a Thermo Finnigan Scorptomatic 1900. The adsorption and desorption of N_2 on the degassed catalyst surfaces was carried out in a vacuum chamber at the temperature of liquid nitrogen (−196 °C) and the specific surface area was determined based on Brunauer–Emmet–Teller (BET) theory. TPD-NH_3 was performed by using a Thermo Finnigan TPD/R/O 1100 instrument equipped with a thermal conductivity detector (TCD). Pretreated catalysts were exposed to NH_3 for an hour at ambient temperature to allow adsorption of the respective gas onto the surfaces. During analysis, the temperature was increased gradually from 50 °C to 850 °C, thus the desorption of NH_3 was simultaneously analysed by TCD under helium flow at a rate of 30 ml min^{-1}.

Deoxygenation reaction

The DO reaction of oleic acid was carried out in a simple glass reactor equipped with a temperature detector and a stirrer (Fig. 1). Approximately 10.0 g of oleic acid was mixed with the catalyst in the reactor and the mixture was heated using a predetermined time and temperature. After the reaction, the product was collected and characterised by using gas chromatography-mass spectroscopy (GCMS) for the purpose of compound composition identification, as well as gas chromatography-flame ionisation detector (GC-FID) for yield and selectivity determination.

Product analysis

The product was analysed by GCMS analyser in order to determine the composition of each sample. The GCMS analyser (Shimadzu QP2010) was equipped with a thermal conductivity detector and a 30.0 m × 0.25 μm × 0.25 mm packed column of RTX-5MS. The sample, dissolved in hexane, Merck GC grade (≥98%), was injected into the column at a temperature of 250 °C. The carrier gas used was helium with a flow rate of 0.80 ml min^{-1}. Initially, the column temperature was set to 50.0 °C and increased gradually to 300 °C at a ramp rate of 3 °C min^{-1}. It was then held for 30 min at the final temperature and the peaks were analysed and identified using the National Institute of Standards and Testing-11 (NIST11) library. GC-FID analysis was carried out in order to determine the total *n*-(C_8–C_{20}) hydrocarbon yield and product selectivity. A GC-FID analyser (Agilent technologies 7890 A) was equipped with a HP5 capillary column with 30 m length, 0.25 mm thickness and 0.25 μm internal diameter. CH_3Br was used as the internal standard, and a saturated and unsaturated hydrocarbon standard was used as the standard. A 1.0 μl aliquot of sample was injected into the GC column at a temperature of 250 °C. Helium served as the carrier gas with a flow rate of 50 ml min^{-1}. The initial temperature of the oven was set at 40 °C and held for 6 min, then ramped up to 260 °C at a heating rate of 7 °C min^{-1}. The programme setting of the GC oven was also supported by several reports.[29–32] The total product after DO reaction (*X*); deoxygenized and intermediates, including acids, ketones, alcohols and aromatic compounds (based on GCMS analysis); and total hydrocarbon yield (*Y*), saturated and unsaturated hydrocarbons including alkenes and alkanes (based on GC-FID analysis), were determined by using eqn (1) and (2).

$$X = \frac{\sum a_o}{\sum a_t} \times 100\% \quad (1)$$

$$Y = \frac{\sum a_n + \sum a_m}{\sum a_o} \times 100\% \quad (2)$$

where a_o = area of reacted products (deoxygenized and intermediates) and a_t = total area of reacted and unreacted (oleic acid) products, while a_n = area of alkenes, and a_m = area of alkanes.

The selectivity (*S*) of the hydrocarbon product (based on GC-FID analysis) was determined by using eqn (3).

$$S(\%) = \frac{n_o}{\sum a_o} \times 100\% \quad (3)$$

where, n_o = area of the selected range of carbon number; gasoline: C_8–C_{12}, diesel: C_{13}–C_{20}.

Optimization by RSM

The DO reaction of oleic acid was implemented and optimized using response surface methodology (RSM) in conjunction with central composite design (CCD) designated by Design-Expert software 8.0.6 (Stat-Ease Inc., USA). The three distinguished factors (independent variables) are *A*: reaction temperature (250–350 °C), *B*: reaction time (1–3 h) and *C*: catalyst amount (1–5 wt%), whereas the identified responses (dependent variable) were the *R*1: yield (%) of the oleic acid to renewable diesel as well as the selectivity towards the formation of *R*2: gasoline (%) and *R*3: diesel (%). The factorials, axial points and centre points coded for the three-levels distinguished parameters are tabulated in Table 2, where they are coded to two levels of factor min = −1 and max = +1, while the two axial points are denoted as +α and −α and the center point as 0.

Table 3 presents the full design matrix of the experiments and results in accordance with the factors of CCD design and

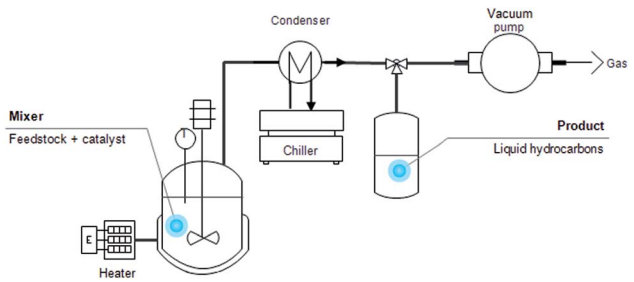

Fig. 1 Schematic diagram of DO reaction.

Table 2 Five-level-three-factor central composite design with the DO condition parameters

	Code	Unit	$-\alpha$	-1	0	+1	$+\alpha$
Temperature	*A*	°C	250	275	300	325	350
Time	*B*	h	1	1.5	2	2.5	3
Catalyst amount	*C*	wt%	1	2	3	4	5

the RSM response values obtained from the experiments. The interaction of the independent variables (*A*, *B*, *C*) can determine the responses of the DO reaction: *R*1, *R*2 and *R*3. Furthermore, these values gives optimum point values of the respective responses in their optimum conditions (parameters). Owing to the simultaneous response obtained for *R*2: gasoline and *R*3: diesel (*R*2 + *R*3 = 100%), only the *R*3 model will be discussed. Response surfaces were designed from quadratic polynomial equation as well as the contour plots obtained from the equation. The model design generates 20 runs of experiment for each catalyst in this study, which comprises eight factorial points, six axial points and six replicates of centre points.

Results and discussion

Characterization of the catalyst

Based on the XRD patterns (see Fig. 2), the peak for fresh Gm comprised cellulose, $(C_6H_{10}O_5)_n$, which is derived from plants and was exhibited in the range of $2\theta = 20–25°$ (JCPDS file no.: 00-050-2241).[33] Small and sharp peaks were also discovered at 27°, 31° and 32° which corresponded to the presence of acetyl methylurea ($C_4H_8N_2O_2$). The presence of a very broad yet low intensity peak at $2\theta = 20–25°$ (JCPDS file no.: 00-050-0926), shown in Fig. 2(ii), proved that activated carbon (Gm) formed after calcination at 500 °C. Simultaneously, the XRD peaks of acetyl methylurea disappeared, indicating that it was decomposed. Fig. 3 shows the elemental composition of Gm analysed by EDX. Based on the spectra, it reveals the existence of other elements, including Ca, Mg, K, Si, Fe and Zr with major percentage <10%. The weak intensities of the EDX spectra for those elements corroborates the absence of their peaks in the XRD profiles. It has been agreed that the detection limit of XRD analysis for phase mixtures is >10.

The Ni–Al HT catalyst resulted in intense peaks at $2\theta = 37.3°$, 43.4° and 63.2°, which belong to cubic NiO at the (111), (200), (220), (311) and (222) planes.[34] All Gm/Ni–Al catalysts exhibit similar peaks with Ni–Al catalyst, suggesting that the presence of Gm did not alter or interrupt the structure of hydrotalcite. However, the intensity of the peaks was reduced as the ratio of Gm : Ni–Al increased owing to a lesser amount of high crystallinity of NiO. The lower intensity of the Gm/Ni–Al series also signifies a good dispersion of Gm on the surface of Ni–Al. Besides, the XRD phase of amorphous aluminium oxide was invisible owing to the merging of aluminium into the lattice of NiO, which happened due to the smaller Al^{3+} ion as compared to Ni^{2+} ion.[35]

The crystallite size of the hydrotalcite catalyst was calculated by using the Debye–Scherrer equation based on the highest intense peak centered at $2\theta = 43.2°$ (Table 4). The crystallite sizes of all materials can be prescribed as in the following order: Gm/Ni–Al 1 : 3 (1.2 nm) ~ Ni–Al (1.5 nm) ~ Gm/Ni–Al 1 : 1 (1.6 nm) < Gm/Ni–Al 3 : 1 (2.4 nm). A smaller crystallite size is proposed to prevent coke formation during the DO process.[36]

The BET surface area and porosity profile of the catalysts are tabulated in Table 4. The surface area of Ni–Al was lower than Gm-incorporated hydrotalcite catalysts and it increased

Table 3 Design matrix and responses of the experiments

	Factors			Responses		
Type	*A*: Temperature (°C)	*B*: Time (h)	*C*: Catalyst amount (wt%)	*R*1: Yield (%)	*R*2: Gasoline (%)	*R*3: Diesel (%)
Factorial	275	1.5	2	85.3	14.0	86.0
Factorial	325	1.5	2	81.3	28.1	71.9
Factorial	275	2.5	2	99.1	19.6	80.4
Factorial	325	2.5	2	85.8	33.5	66.5
Factorial	275	1.5	4	93.3	25.6	74.4
Factorial	325	1.5	4	89.2	34.9	65.1
Factorial	275	2.5	4	98.2	27.4	72.6
Factorial	325	2.5	4	87.2	37.5	62.5
Axial	250	2	3	97.3	13.9	86.1
Axial	350	2	3	78.3	39.8	60.2
Axial	300	1	3	93.1	25.8	74.2
Axial	300	3	3	96.2	33.2	66.8
Axial	300	2	1	88.7	20.9	79.1
Axial	300	2	5	98.1	33.7	66.3
Center	300	2	3	96.1	30.4	69.6
Center	300	2	3	92.7	27.7	72.3
Center	300	2	3	95.4	31.1	68.9
Center	300	2	3	93.6	30.7	69.3
Center	300	2	3	93.1	28.3	71.7
Center	300	2	3	95.7	29.9	70.1

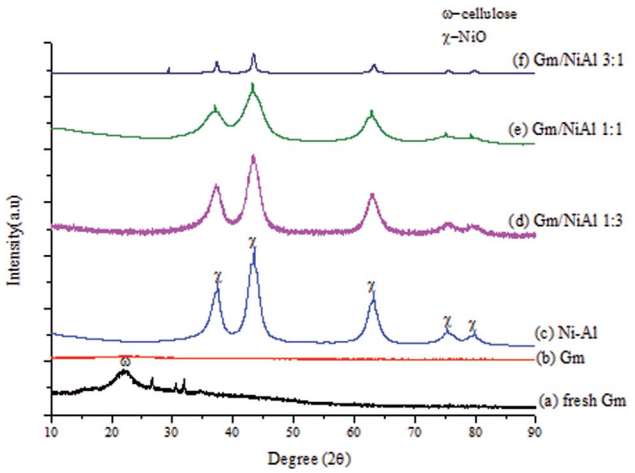

Fig. 2 (i) XRD profiles of (a) fresh Gm, (b) Gm, (c) Ni–Al, (d) Gm/NiAl 1 : 3, (e) Gm/NiAl 1 : 1, (f) Gm/NiAl 3 : 1, and (ii) XRD pattern for Gm.

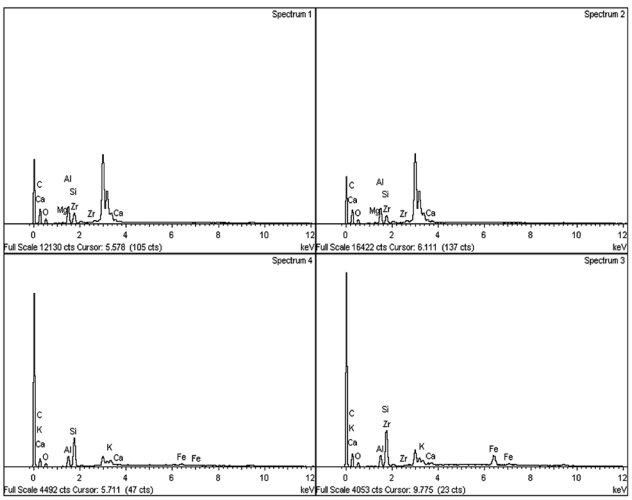

Fig. 3 EDX elemental profiles of Gm.

following order of Gm < Ni–Al < Gm/Ni–Al 1 : 3 < Gm/Ni–Al 1 : 1 < Gm/Ni–Al 3 : 1. The increase in surface area was attributed to the incorporation of Ni–Al on the Gm support, where sonication of this gelatinous precipitate during the synthesis was able to disperse the coagulated precipitate homogeneously. It was found that surface area does not show any significant correlation with the crystallite size of the catalyst (refer to XRD result). In the case of the catalysts' porosity, all Gm-incorporated catalysts resulted in enlargement of the pore diameter from 4.6 nm (Ni–Al) to 9.9–14.6 nm (Gm/Ni–Al), indicating that the catalysts mainly consist of a dead-end mesoporous (2–50 nm) structure. This result was in agreement with the large pore size of Gm (27.8 nm). Meanwhile, the pore volume follows a trend: Gm > Gm/Ni–Al 3 : 1 > Gm/Ni–Al 1 : 1 > Gm/Ni–Al 1 : 3 > Ni–Al. The substantial increment of the pore volume of Gm/Ni–Al catalyst was likely correlated with narrow porosity or hollow core cavities, thus resulting in high surface area. The higher surface area of the Gm/Ni–Al series corroborates with the XRD results, which show good dispersion of Ni–Al on the Gm support. Based on the results, it can be assumed that the Gm/Ni–Al catalyst with high surface area has high potential for promoting the DO reaction due to the wide channel accessibility of the reactant and product to the catalyst's active sites.

The changes to the surface morphology for the Gm-incorporated Ni–Al catalyst were determined by FESEM analysis (Fig. 4). The typical Ni–Al catalyst shows a rough surface with irregular shapes of particles (see Fig. 4a). The pore structure was not clearly seen, suggesting that a wide pore diameter (refer to BET) was determined from the shallow pores of the Ni–Al catalyst. The FESEM morphology for each Gm/Ni–Al catalyst displays the regeneration of multilayer surfaces resulting from incorporation of the Gm support (Fig. 4b–d). Gm/Ni–Al 1 : 3 shows multilayers of flat surface with no obvious pore structure. However, the apparent pore structure was exposed by Gm/Ni–Al 1 : 1 (see Fig. 4c) and Gm/Ni–Al 3 : 1 (see Fig. 4d), which correlated with the enhancement of the BET surface area of each catalyst. Gm displays a smooth surface with the presence of a pore structure, in agreement with the study reported by Hajati *et al.*[37] It could be summarized that Gm/Ni–Al has emulated the rough surfaces and porosity of both Ni–Al and Gm, concurrently. The Gm/Ni–Al textural properties are proposed to alleviate the DO reaction of oleic acid.

The acidity profile of Gm/Ni–Al, Ni–Al and Gm catalysts was studied by TPD-NH_3 analysis (Table 4 and Fig. 5). All catalysts exhibits NH_3 desorption peak >500 °C, which attributed to strong acid strength of active sites.[38] Among the catalysts, Gm rendered the lowest acid density (288.81 μmol g^{-1}) owing to the absence of oxygen-containing surface lattice, which was attributed to the decomposition of oxygenous compounds in Gm during the thermal activation process.[39] Based on the acid distribution profile, the Ni–Al catalyst rendered strongest acid strength (635 °C) with a total acidity of 6050.22 μmol g^{-1}, which resulted from the Lewis acid sites of the Ni^{2+}–O^{2-} pair. The presence of Al with

Table 4 Crystallite sizes, textural properties and acidity profiles of hydrotalcite catalysts

	XRD	BET			TPD-NH_3	
Catalyst	Crystallite size[a] (nm)	Surface area[b] (m^2 g^{-1})	Pore diameter[b] (nm)	Pore volume[b] (cc g^{-1})	NH_3 desorption temperature[c] (°C)	Total amount of NH_3 desorbed[c] (μmol g^{-1})
Ni–Al	1.5	116.8	4.6	0.21	635	6050.22
Gm/Ni–Al 1 : 3	1.2	166.3	9.9	0.46	603, 768	10 636.35
Gm/Ni–Al 1 : 1	1.6	183.6	13.6	0.50	579, 755	17 290.73
Gm/Ni–Al 3 : 1	2.4	190.7	14.6	0.70	565	1122.26
Gm	—	68.1	27.8	0.71	583	288.81

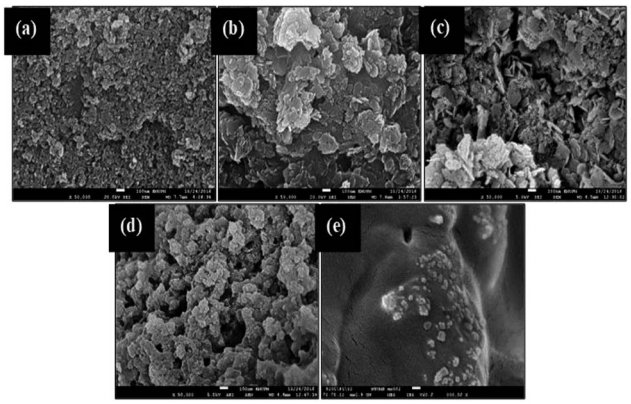

Fig. 4 FESEM image of (a) Ni–Al (b) Gm/Ni–Al 1 : 3 (c) Gm/Ni–Al 1 : 1 (d) Gm/Ni–Al 3 : 1 and (e) Gm catalysts.

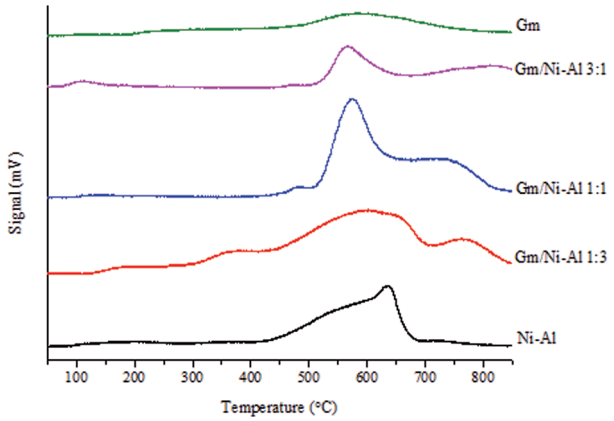

Fig. 5 TPD-NH_3 profiles for synthesized catalysts.

amphoteric properties enhanced the interaction and acidity of Ni–Al. Meanwhile, Gm/Ni–Al 1 : 1 showed the highest acid density among Gm-incorporated Ni–Al catalysts with a total acidity of 17 290.73 μmol g^{-1}. It was strongly suggested that strong interaction of Gm with Ni–Al species was dynamically achieved with a 1 : 1 ratio, which actuates the synergetic effect that further intensifies the acidity of the catalyst.[40]

Catalytic deoxygenation

The hydrocarbon yield and total product profile of the catalytic DO reaction are shown in Fig. 6a. Gm/Ni–Al catalysts give high catalytic activity towards DO reaction with a hydrocarbon yield of 90.3–98.1% and total product yield of 98.1–99.9%. Among the Gm-incorporated Ni–Al catalysts, the highest hydrocarbon yield was obtained by using the Gm/Ni–Al 1 : 1 catalyst, which resulted in a 98.1% hydrocarbon yield and a 99.9% total product yield. It is strongly suggested that the catalytic activity towards the DO reaction of the Gm/Ni–Al 1 : 1 catalyst was enhanced owing to its high acid density (refer to TPD-NH_3 results). Apart from the enriched acid characteristic, the textural properties of the Gm/Ni–Al 1 : 1 catalyst were also improved (refer to BET results). Individually, Ni–

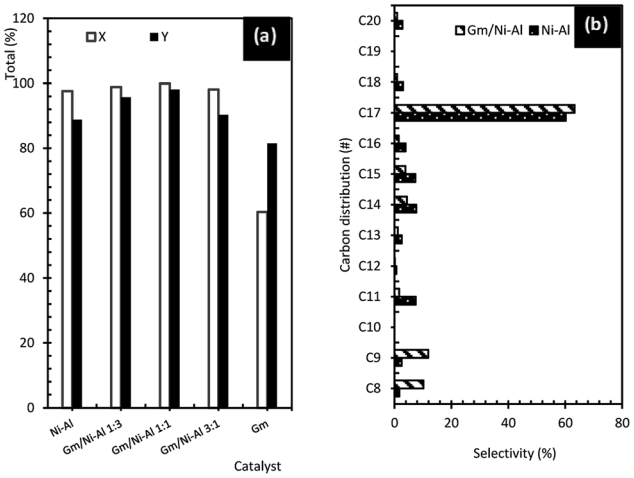

Fig. 6 (a) Total of product and hydrocarbon yield, and (b) product selectivity of liquid deoxygenated product.

Al resulted in an 88.8% hydrocarbon yield and a 97.6% total converted product yield. This was due to the number of acid sites of the Ni–Al catalyst, which facilitates the DO reaction. Besides, it was proposed that Ni–Al has cracking ability, which can avoid coke formation during the reaction.[41,42] The activity of Gm showed the lowest hydrocarbon yield and total product yield, with 81.5% and 60.3%, respectively. This correlates with the lowest amount of acid sites and the absence of an oxygen-functioning surface, which is favourable for catalytic reaction.[39]

Stimulatingly, it was speculated that the existence of a limited quantity of acid–base elements, such as Mg, Ca, Si, Fe and Zr (refer to EDX results) in Gm improves the performance of the Gm/Ni–Al catalyst, and hence enhances the activity of removal of oxygenates through the DO reaction. Evidently, previous studies have found that active metals with acid/base properties as well as stable morphological characteristics, Mg, Ca and Zr, facilitate C–O cleavage through the decarboxylation and decarbonylation pathways.[43–45] Consequently, Gm-incorporated Ni–Al catalyst resulted in higher selectivity towards C_{17} (*n*-heptadecene and *n*-heptadecane), C_9 (*n*-nonane and *n*-nonene), and C_8 (*n*-octane and *n*-octene), indicating that incorporation of Gm species onto the Ni–Al catalyst enhanced the product selectivity owing to better textural characteristics and a synergistic effect in acidic properties (see Fig. 6b). Therefore, the DO reaction of oleic acid *via* Gm/Ni–Al 1 : 1 catalyst was further optimized by using RSM analysis.

Optimization by RSM

Validation of model regression. A quadratic polynomial equation was selected for designing the response surfaces as well as the contour plots for each interaction owing to it having the highest order polynomial, significant additional terms and no aliased model. The results for *R*1: yield and *R*3: diesel selectivity responses for Gm/Ni–Al catalytic DO, analysed by ANOVA, are tabulated in Table 5. Based on the results, there were significant effects of interactions among the individual variables as well as between different variables to that of the responses. It shows that Gm/Ni–Al catalyst has Prob > *F* values

of 0.0004 for the $R1$ model and <0.0001 for the $R3$ model, which indicates that both models were significant ($p < 0.05$). The significant model terms were $R1 = A, B, C, AB, BC, A^2$, while $R3 = A, B, C, AC, A^2$ and C^2. Besides, insignificant F-values of lack of fit indicate that the $R1$ and $R3$ model were well-fitted. The coefficient of variation (CV) values were less than 10% with a high degree of precision, proposing that the data sets of the experiments were reliable with $R1 = 2.62\%$ and $R3 = 1.66\%$. The result was also in line with the R^2 value of the data experiments, with values of 0.9104 and 0.9845 for $R1$ and $R3$, respectively. It should be noted that a perfect regression line will have an R^2 value of 1, whereas an R^2 of 0 means that the regression line is not fit at all. Moreover, adequate precision has a value of more than 4, which shows a high signal to noise ratio, thus the model can be used to conduct the design of study.

According to the ANOVA results obtained from the Gm/Ni–Al catalysed DO reaction, the suggested model terms that have a positive impact on $R1$ were B, C and AC. This indicates that any differences of distinguished parameters B and C as well as the interactions between A and C would have a positive influence on the $R1$. On the other hand, A, AB and A^2 showed negative feedback to $R1$, resulting in a decrement of yield, whereas AC, B^2 and C^2 do not have a significant impact on $R1$. Meanwhile, the suggested model terms that have a positive effect on $R3$ were AC, BC, A^2, and C^2. On the contrary, A, B and C parameters resulted in a negative response in $R3$, while no significant effect was given by the AB and B^2 interactions.

Interaction effects of reaction parameters on DO reaction towards responses. RSM software demonstrated that the incorporation of reaction temperature: A, time: B and catalyst amount: C gave a significant impact on the $R1$: yield as well as $R2$: gasoline and $R3$: diesel selectivity of the oleic acid DO reaction. The six replication models of experiments, which confirm the good probability of the data set, are shown as red points in the middle of the 3D and 2D plots. In the 3D surface plots, the vertical axis represents any increment of percentage of yield and diesel, while the two horizontal axes represent the respective parameters of the DO reaction. Based on the RSM 2D contour and 3D surface plots, the red point revealed in the middle of both plots indicates the good predictability of the design, which has been replicated six times.

Interaction effect between temperature and catalyst amount (A–C) towards R1: yield. The response for the interaction between A: temperature and C: catalyst amount towards the DO reaction for Gm/Ni–Al catalyst is exhibited in the 3D surface and 2D contour plots (see Fig. 7a and b). B: reaction time was fixed at 2 h.

The 3D surface plot shows an increase of hydrocarbon yield on one axis, whereas another axis remains at a low level for reaction temperature or catalyst amount. The interaction between temperature and catalyst amount resulted in a plateau effect, since the reaction reached an equilibrium when the catalyst amount used was 5 wt%. The result was in agreement with the 2D contour plot in which the reaction model favoured a high hydrocarbon yield at an intermediate level of temperature (250–300 °C) with a maximum 5 wt% of catalyst. Catalyst amount played a vital role in triggering and enhancing the catalytic activity of the Gm/Ni–Al catalysed DO reaction.

Increasing the catalyst amount resulted in a high hydrocarbon yield at an intermediate level of temperature. On the contrary, increment of temperature does not increase the catalytic activity at the maximum amount of catalyst. The DO reaction at a temperature of 250 °C gives ~92% yield and the percentage was increased to 96.6% with the addition of catalyst amount to 5 wt% at the same reaction temperature. At this point, more catalyst provides more accessible surfaces for the DO reaction of oleic acid. Using the same amount of catalyst at

Table 5 Analysis of variance (ANOVA) for $R1$ and $R3$ of Gm/Ni–Al catalyst model regression

Anova	$R1$: Yield		$R3$: Diesel	
	p-Value		p-Value	
Model	0.0004	Significant	< 0.0001	Significant
A-Temperature (°C)	< 0.0001		< 0.0001	
B-Time (h)	0.0179		< 0.0001	
C-Catalyst amount (wt%)	0.0044		< 0.0001	
AB	0.0381		0.8625	
AC	0.7514		0.0287	
BC	0.0482		0.0768	
A^2	0.0028		0.0087	
B^2	0.7070		0.6565	
C^2	0.3242		0.0198	
Predicted $R1$ equation with significant factors	$= +93.95 - 4.41A + 1.70B + 2.21C - 2.03AB + 0.28AC - 1.92BC - 1.89A^2 - 0.19B^2 - 0.50C^2$		$= +70.48 - 6.20A - 1.90B - 3.48C - 0.075AB + 1.08AC + 0.83BC + 0.77A^2 + 0.11B^2 + 0.66C^2$	
Lack of fit	0.0653	Not significant	0.7577	Not significant
Std. Dev.	2.41		1.19	
Mean	91.89		71.71	
CV%	2.62		1.66	
R-squared	0.9104		0.9845	
Adj R-squared	0.8298		0.9705	
Adeq precision	12.891		29.402	

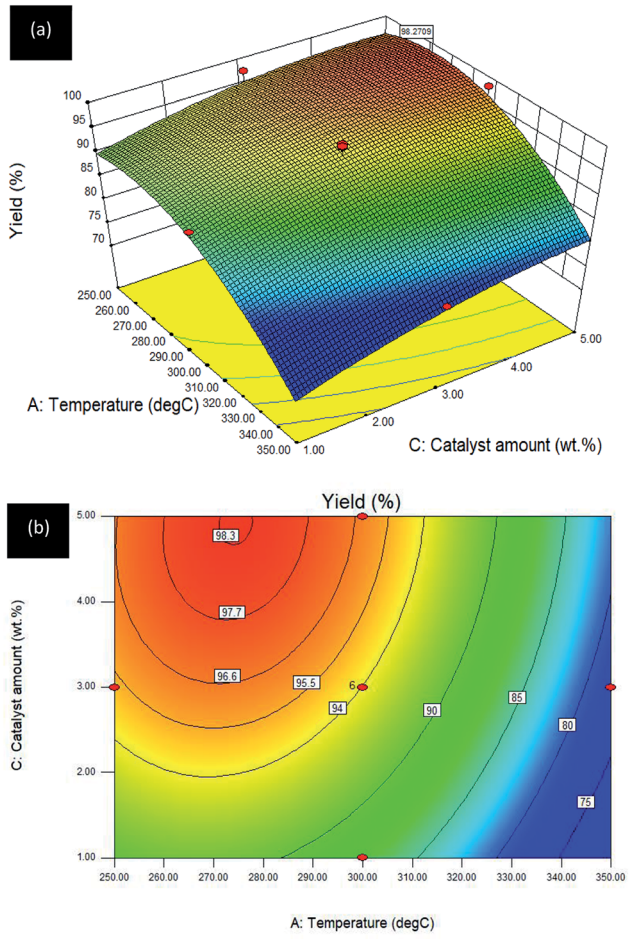

Fig. 7 (a) 3D image and (b) 2D image of RSM interaction effects between *A*: temperature and *C*: catalyst amount for Gm/Ni–Al catalysed reaction on *R*1: yield; reaction condition: reaction time = 2 h.

a higher temperature (~275 °C) would maximise the yield to 98.3% and the percentage yield returned to 96.6% when the temperature reached 300 °C. At this temperature, the yield decreased to ~87% as the catalyst amount was reduced to 1 wt%. The percentage yield gradually declined as the temperature was intensified to 350 °C with <80% of yield. It can be concluded that the interaction of temperature–catalyst can be maximised with sufficient amount of catalyst and by controlling the temperature.

Temperature–catalyst amount (A–C) interaction effect towards R3:diesel. The effect of A: temperature and C: catalyst amount on diesel selectivity (reaction time was kept constant at 2 h) for the Gm/Ni–Al catalysed DO reaction is revealed in the 3D surface plot (see Fig. 8a) and the 2D contour plot (see Fig. 8b).

An inverted curvilinear effect occurred in the 3D surface plot owing to the decrement in Gm/Ni–Al catalyst amount giving a remarkable increase in diesel yield between the initial and intermediate range (250–325 °C). However, there was a slight increment as the catalyst amount reached its limit (3–5 wt%) at the highest temperature (335–350 °C). The 2D contour plot depicted high diesel selectivity at the low reaction temperature (250–280 °C) and low catalyst amount (1–3 wt%). It can be summarized that the Gm/Ni–Al catalysed reaction only requires low temperature and a small amount of catalyst for highest diesel selectivity. Further increment in temperature resulted in reaction drawbacks and over-cracking of oleic acid.[46]

Time–catalyst amount (B–C) interaction effect towards R3:diesel. The influence of the interaction between *B*: time and *C*: catalyst amount, while temperature was fixed at 300 °C, on diesel selectivity of the DO reaction *via* Gm/Ni–Al catalyst is depicted in 2D contour and 3D surface plots (see Fig. 9).

Similar to Fig. 7, the 3D surface plots also exhibited an overturned curvilinear shape in which higher diesel selectivity was achieved with the reduced catalyst amount within a short reaction time. However, the diesel selectivity was slightly increased as the reaction time reached its highest level (2.6–3.0 h) with the corresponding maximum limit of catalyst amount (4.5–5.0 wt%). Over 80% diesel selectivity was obtained by using <2.0 wt% catalyst amount with 1.40 h reaction time. The maximum diesel selectivity was obtained using 1 wt% of catalyst and 1 h reaction time. It can be summarized that prolonged reaction time would be detrimental, even though the catalyst amount is increased. This is owing to a high opportunity for catalysed deoxygenation of oleic acid into gasoline, instead of diesel, under this reaction condition: temperature of 300 °C.[47]

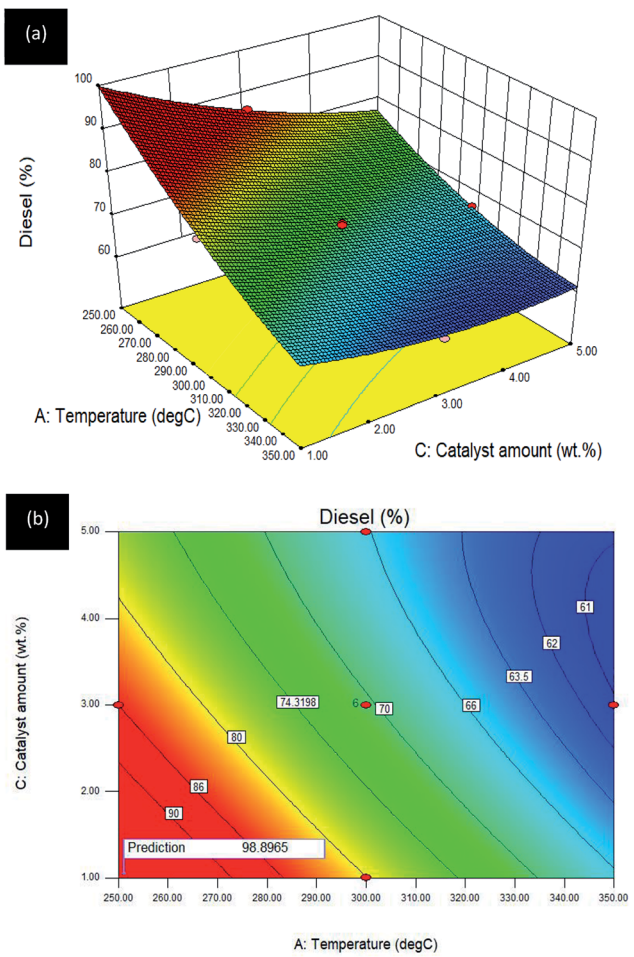

Fig. 8 (a) 3D image and (b) 2D image of RSM interaction effects between *A*: temperature and *C*: catalyst amount for Gm/Ni–Al catalysed reaction on *R*3: diesel; reaction condition: reaction time = 2 h.

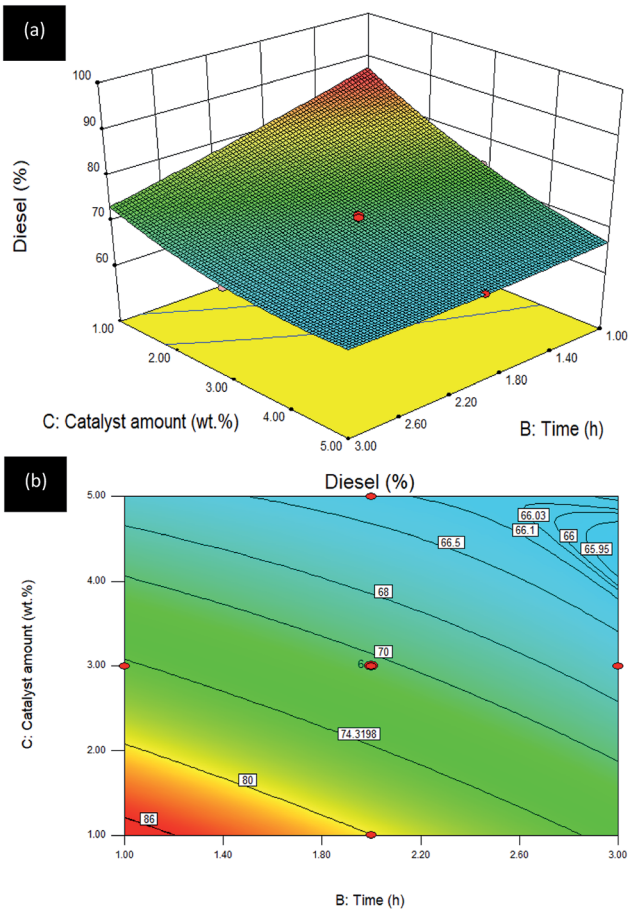

Fig. 9 (a) 3D image and (b) 2D image of RSM interaction effects between *B*: time and *C*: catalyst amount for Gm/Ni–Al catalysed reaction on *R*3: diesel; reaction temperature = 300 °C.

Generally, a high temperature was required for the DO reaction of oleic acid, suggesting that the viscosity of the reactant was reduced, thus increasing oleic acid diffusion with catalyst. However, overheating resulted in over-cracking of oleic acid, suggesting that more gaseous and short-chained hydrocarbons were produced. The hydrocarbon yield decreased at higher reaction temperature owing to the formation of intermediate hydrocarbons, such as ketones and aldehydes.

Prolonged reaction time increased the hydrocarbon yield owing to sufficient time being provided. However, it must be mentioned that the viscosity of the reactants would increase by prolonging the reaction time. At this point, some reactants would crack to gasoline. Sufficient catalyst amount provides more surfaces for greater accessibility of oleic acid. The optimum catalyst amount used gives a high yield of product, correlating that the catalyst improves conversion by providing active sites for the DO reaction.[41,48]

Optimizing operating conditions for Gm/Ni–Al catalysed deoxygenation reaction. In order to determine the optimum operating conditions for the Gm/Ni–Al catalysed DO reaction, it was crucial to set the variables (temperature, time and catalyst amount) in the range of high to low levels, coded as −1 and +1. Targeted values for all responses were fixed as desired: maximum yield, minimum gasoline and maximum diesel selectivity. Table 6 tabulates the optimized reaction conditions and point prediction results for the Gm/Ni–Al catalysts and responses. Based on all the reaction conditions, the lower and upper limits are the minimum and maximum responses obtained during the experiments. The upper limit of *R*1: yield was 99.1%, while *R*3: diesel was 86.1%. The optimum conditions for the Gm/Ni–Al catalysed DO reaction were temperature: 327.14 °C, time: 1 h and catalyst: 5.0 wt%. With these reaction conditions, it was predicted to produce a 97.9% of hydrocarbon yield with 70.4% diesel selectivity. However, results from the experiment exhibited a minor deviation in diesel selectivity, which produced 70.4% diesel, despite a minor difference in yield of less than 5%. It can be summarized that the generated quadratic model is reliable for the Gm/Ni–Al catalysed DO reaction since it shows good precision and predictability for all responses, corresponding to the optimum operating conditions.

Table 6 (a) Optimization criteria for all reaction parameters and (b) results of all studied responses on model validation at optimum levels

(a)

		Gm/Ni–Al	
Name	Goal	Lower limit	Upper limit
A: Temperature (°C)	Is in range	250	350
B: Time (h)	Is in range	1	3
C: Catalyst amount (wt%)	Is in range	1	5
*R*1: Yield (%)	Maximize	78.3	99.1
*R*2: Gasoline (%)	Minimize	13.9	39.8
*R*3: Diesel (%)	Maximize	60.2	86.1

(b)

Response	*A*: Temp (°C)	*B*: Time (h)	*C*: Catalyst (wt%)	Prediction	Experimental
Yield	327.14	1	5	97.9	94.4
Gasoline				36.3	29.7
Diesel				63.7	70.4

Conclusion

Gm/Ni–Al 1 : 1 catalysed DO of oleic acid into paraffinic hydrocarbons was successful owing to its high total acidity (17 290.73 μmol g^{-1}) and high surface area (183.6 m^2 g^{-1}) as compared to other catalysts with ratios of Gm/Ni–Al 3 : 1 and Gm/Ni–Al 1 : 3. Bio-hydrocarbon at C_{17} (heptadecane and *n*-heptadecene) was the major component found in the deoxygenated liquid. The results indicate that the characteristics of goat manure-derived activated carbon rendered a significant effect towards hydrocarbon productivity and selectivity. The catalyst with acidity–basicity provides better selectivity for renewable fuel (diesel: C_{13}–C_{20}), while the product yield was optimised by the higher surface area and porosity of the catalyst. Besides, the acidic properties of the Gm/Ni–Al catalyst offer higher conversion owing to the presence of cracking pathway that is generated from the acid sites of the catalyst, as well as the

favourable decarboxylation pathway of oleic acid on the mildly basic sites of the hydrotalcite itself. Based on the RSM reaction model regression of the Gm/Ni–Al catalysed DO process, the optimum hydrocarbon yield was 97.9% with 63.7% diesel selectivity at its optimum reaction conditions; reaction temperature: 327.14 °C, reaction time: 1 h, and catalyst amount: 5 wt%.

Conflicts of interest

The authors declare no conflict of interest, financial or otherwise.

Acknowledgements

The authors acknowledge financial support from the University Malaysia (GC001B-14AET, ST014-2017 and ST012-2018), the Postgraduate Research Grant Scheme PPP (PG062-2015A) and MyPhD scholarship from Ministry of Education, Malaysia.

References

1 E. Y. Emori, F. H. Hirashima, C. H. Zandonai, C. A. Ortiz-Bravo, N. R. C. Fernandes-Machado and M. H. N. Olsen-Scaliante, *Catal. Today*, 2017, **279**, 168–176.
2 M. A. Machado, S. He, T. E. Davies, K. Seshan and V. Teixeira da Silva, *Catal. Today*, 2018, **302**, 161–168.
3 A. Kumar, K. Iwatani, S. Nishimura, A. Takagaki and K. Ebitani, *Catal. Today*, 2012, **185**, 241–246.
4 D. A. Bulushev and J. R. H. Ross, *Catal. Today*, 2011, **171**, 1–13.
5 P. Grange, E. Laurent, R. Maggi, A. Centeno and B. Delmon, *Catal. Today*, 1996, **29**, 297–301.
6 E. Sendzikiene, V. Makareviciene and P. Janulis, *Renewable Energy*, 2006, **31**, 2505–2512.
7 S. K. Tanneru and P. H. Steele, *Renewable Energy*, 2015, **80**, 251–258.
8 E. Santillan-Jimenez, T. Morgan, J. Shoup, A. E. Harman-Ware and M. Crocker, *Catal. Today*, 2014, **237**, 136–144.
9 E.-M. Ryymin, M. L. Honkela, T.-R. Viljava and A. O. I. Krause, *Appl. Catal., A*, 2010, **389**, 114–121.
10 P. Kittisupakorn, S. Sae-ueng and A. Suwatthikul, in *26th European Symposium on Computer Aided Process Engineering*, ed. Z. Kravanja and M. Bogataj, Elsevier, 2016, vol. 38, pp. 751–756.
11 Y. Yang, Q. Wang, X. Zhang, L. Wang and G. Li, *Fuel Process. Technol.*, 2013, **116**, 165–174.
12 K. C. Kwon, H. Mayfield, T. Marolla, B. Nichols and M. Mashburn, *Renewable Energy*, 2011, **36**, 907–915.
13 A. T. Madsen, B. Rozmysłowicz, I. L. Simakova, T. Kilpiö, A.-R. Leino, K. Kordás, K. Eränen, P. Mäki-Arvela and D. Y. Murzin, *Ind. Eng. Chem. Res.*, 2011, **50**, 11049–11058.
14 O. B. Ayodele, H. F. Abbas and W. M. A. W. Daud, *Energy Convers. Manage.*, 2014, **88**, 1111–1119.
15 O. V Kikhtyanin, A. E. Rubanov, A. B. Ayupov and G. V Echevsky, *Fuel*, 2010, **89**, 3085–3092.
16 O. B. Ayodele and W. M. A. W. Daud, *J. Taiwan Inst. Chem. Eng.*, 2015, **47**, 113–124.
17 N. Asikin-Mijan, H. V Lee, J. C. Juan, A. R. Noorsaadah, G. Abdulkareem-Alsultan, M. Arumugam and Y. H. Taufiq-Yap, *J. Anal. Appl. Pyrolysis*, 2016, **120**, 110–120.
18 B. Puértolas, T. C. Keller, S. Mitchell and J. Pérez-Ramírez, *Appl. Catal., B*, 2016, **184**, 77–86.
19 H. Tani, T. Hasegawa, M. Shimouchi, K. Asami and K. Fujimoto, *Catal. Today*, 2011, **164**, 410–414.
20 H.-Y. Zeng, S. Xu, M.-C. Liao, Z.-Q. Zhang and C. Zhao, *Appl. Clay Sci.*, 2014, **91–92**, 16–24.
21 H. T. Kang, K. Lv and S. L. Yuan, *Appl. Clay Sci.*, 2013, **72**, 184–190.
22 J. F. P. Gomes, J. F. B. Puna, L. M. Gonçalves and J. C. M. Bordado, *Energy*, 2011, **36**, 6770–6778.
23 J. Kong, L. Jiang, Z. Huo, X. Xu, D. G. Evans, J. Song, M. He, Z. Li, Q. Wang and L. Yan, *Catal. Commun.*, 2013, **40**, 59–62.
24 M. Radlik, M. Motak, M. Elena, W. Turek, P. Da and T. Grzybek, *Catal. Today*, 2015, **257**, 59–65.
25 Q. Liu, C. Wang, W. Qu, B. Wang, Z. Tian, H. Ma and R. Xu, *Catal. Today*, 2014, **234**, 161–166.
26 J.-G. Na, B. E. Yi, J. N. Kim, K. B. Yi, S.-Y. Park, J.-H. Park, J.-N. Kim and C. H. Ko, *Catal. Today*, 2010, **156**, 44–48.
27 C. Miao, O. Marin-Flores, S. D. Davidson, T. Li, T. Dong, D. Gao, Y. Wang, M. Garcia-Pérez and S. Chen, *Fuel*, 2016, **166**, 302–308.
28 E. Santillan-Jimenez, T. Morgan, J. Lacny, S. Mohapatra and M. Crocker, *Fuel*, 2013, **103**, 1010–1017.
29 J. Asomaning, P. Mussone and D. C. Bressler, *J. Anal. Appl. Pyrolysis*, 2014, **105**, 1–7.
30 R. Fréty, J. G. A. Pacheco, M. R. Santos, J. F. Padilha, A. F. Azevedo, S. T. Brandão and L. A. M. Pontes, *J. Anal. Appl. Pyrolysis*, 2014, **109**, 56–64.
31 N. Asikin-Mijan, H. V Lee, T. S. Marliza and Y. H. Taufiq-Yap, *J. Anal. Appl. Pyrolysis*, 2018, **129**, 221–230.
32 J. T. Scanlon and D. E. Willis, *J. Chromatogr. Sci.*, 1985, **23**, 333–340.
33 M. Yahya, H. Lee and S. B. Abd Hamid, *Preparation of Nanocellulose via Transition Metal Salt-Catalyzed Hydrolysis Pathway*, 2015, vol. 10.
34 L. Bian, W. Wang and Z. Li, *RSC Adv.*, 2015, **6**, 677–686.
35 S. V Cherepanova, N. N. Leont'eva, A. B. Arbuzov, V. A. Drozdov, O. B. Belskaya and N. V Antonicheva, *J. Solid State Chem.*, 2015, **225**, 417–426.
36 P. Magnoux, A. Rabeharitsara and H. S. Cerqueira, *Appl. Catal., A*, 2006, **304**, 142–151.
37 S. Hajati, M. Ghaedi and S. Yaghoubi, *J. Ind. Eng. Chem.*, 2015, **21**, 760–767.
38 N. Asikin-Mijan, H. V. Lee and Y. H. Taufiq-Yap, *Chem. Eng. Res. Des.*, 2015, **102**, 368–377.
39 M. S. Shafeeyan, W. M. A. W. Daud, A. Houshmand and A. Shamiri, *J. Anal. Appl. Pyrolysis*, 2010, **89**, 143–151.
40 W. Song, Y. Liu, E. Barath, C. Zhao and J. A. Lercher, *Green Chem.*, 2015, **17**, 1204–1218.
41 K. Hengst, M. Arend, R. Pfützenreuter and W. F. Hoelderich, *Appl. Catal., B*, 2015, **174–175**, 383–394.

42 T. B. Čelič, M. Grilc, B. Likozar and N. N. Tušar, *ChemSusChem*, 2015, **8**, 1703–1710.
43 X. Yu, J. Chen and T. Ren, *RSC Adv.*, 2014, **4**, 46427–46436.
44 N. Asikin-Mijan, H. V Lee, Y. H. Taufiq-Yap, J. C. Juan and N. A. Rahman, *J. Anal. Appl. Pyrolysis*, 2016, **117**, 46–55.
45 X. Chen, Y. Chen, H. Yang, X. Wang, Q. Che, W. Chen and H. Chen, *Bioresour. Technol.*, 2019, **273**, 153–158.
46 M. Y. Kim, J.-K. Kim, M.-E. Lee, S. Lee and M. Choi, *ACS Catal.*, 2017, **7**, 6256–6267.
47 C. Zhao, T. Bruck and J. A. Lercher, *Green Chem.*, 2013, **15**, 1720–1739.
48 S. A. Khromova, A. A. Smirnov, S. A. Selishcheva, R. G. Kukushkin, V. O. Dundich, L. I. Trusov and V. A. Yakovlev, *Catal. Ind.*, 2013, **5**, 260–268.